Viscoelastic Properties of Microtubule Networks

Yi-Chia Lin,[†] Gijsje H. Koenderink,[†,‡] Frederick C. MacKintosh,[§] and David A. Weitz*[,†]

Department of Physics and School of Engineering and Applied Sciences, Harvard University, Cambridge, Massachusetts 02138, and Department of Physics and Astronomy, Vrije Universiteit, Amsterdam, The Netherlands

Received April 12, 2007; Revised Manuscript Received July 22, 2007

ABSTRACT: Microtubules are filamentous protein biopolymers found in eukaryotic cells. They form networks that guide active intracellular transport and support the overall cell structure. Microtubules are very rigid polymers, with persistence lengths as large as a millimeter. As such, they constitute an example of rodlike polymers, whose mechanical and rheological properties are as yet poorly understood. We measure the linear and nonlinear viscoelastic properties of isotropic solutions of purified microtubules, as well as networks permanently cross-linked with biotin−NeutrAvidin. In the linear regime both solutions and networks are soft elastic materials with elastic moduli on the order of a few pascals. The elastic moduli show a power-law dependence on tubulin concentration, c_T, with $G' \sim c_T^{\nu}$, where $\nu \approx 1.4$ for solutions and increases slightly to $\nu \approx 1.6-1.8$ for networks. At large deformations, we observe a concentration-dependent yield stress. The rheology of microtubule solutions cannot be explained by the Doi−Edwards model, which treats noninteracting rigid rods. Instead, they show behavior very similar to the permanently cross-linked networks, suggesting the presence of effective cross-linking even in pure microtubule solutions. We develop a simple model based on transient cross-linking interactions between microtubules to interpret the rheological response. We also calculate a lower bound estimate of the strength of this interaction. Our data provide a framework with which to understand the dynamics and mechanics of more physiological networks of microtubules with microtubule-associated cross-linking and motor proteins, and ultimately to understand the role of microtubules in cell mechanics.

Introduction

Cells interact mechanically with their environment through their *cytoskeleton*, a network consisting largely of filamentous protein polymers. Reconstituted solutions and networks of these biopolymers have rich rheological and elastic properties that arise from their semiflexibility, with thermal persistence lengths comparable to or even much larger than their contour length. On the extreme end of polymer stiffness are microtubules, whose persistence length is on the order of 1 mm[1,2] and which form networks for intracellular transport and mechanical support of the cell.[3] While the viscoelastic properties of reconstituted models of other cytoskeletal filaments, most notably F-actin,[4,5] have been widely studied *in vitro*, relatively little is known about the network properties of microtubules. Prior work has focused on the dynamic properties of single filaments[2] and forces generated during microtubule polymerization.[6,7] Since microtubules in cells form networks that can provide structural support and assist in cellular locomotion and transport, it is also important to understand the mechanical properties of networks of microtubules. The mechanical properties of microtubule networks were studied only over a narrow range of tubulin concentrations and over a limited range of frequencies.[8,9] Here, we investigate the viscoelastic properties of microtubule solutions and networks as a function of both concentration and cross-linking.

A microtubule is a stiff, hollow cylinder built from 13 parallel protofilaments, each composed of globular tubulin subunits. Microtubules are the stiffest filaments of the cytoskeleton, with a persistence length of a few millimeters, a contour length $L \sim 10\ \mu$m, and a diameter $D = 25$ nm. *In vitro*, microtubules can be reconstituted from purified tubulin by polymerization in the presence of Mg^{2+} and guanosine triphosphate (GTP). These reconstituted filaments have a very high aspect ratio, $L/D \approx 10^3$. As such, microtubules can provide an excellent model system with which to study the dynamics and rheology of rigid rods. Previous studies of entangled rod solutions have addressed only a limited range of aspect ratios; colloidal rigid rodlike particles usually have an aspect ratio of at most 10[2],[10−12] while biopolymers like fd virus are relatively flexible.[13,14] Furthermore, while most studies of entangled rod solutions have focused on steady shear properties, there have been some studies of the viscoelastic properties.[15,16] In addition, there have been studies of gels and cross-linked networks of rodlike, noncytoskeletal polymers.[17−19]

Here we report the linear viscoelastic properties of microtubule networks measured over an extended frequency range by oscillatory measurements and augmented by creep tests. We also examine the elastic behavior in the nonlinear regime by performing large-amplitude oscillatory stress measurements and by differential measurements of the tangent elastic modulus. We also investigate the viscoelastic properties of networks that are permanently cross-linked by irreversible biotin−NeutrAvidin bonds. We compare our data to existing theoretical predictions and show that the solution data cannot be explained by the Doi−Edwards model,[20] which assumes high aspect ratio, noninteracting rigid rods. Combining these data with the similar data for cross-linked networks, we hypothesize that there are weak attractive interactions between microtubule filaments and we develop a simple model to interpret the viscoelastic response of both solutions and networks. As further evidence for attractive interactions and effective cross-linking of solutions, we observe a yield stress similar to that of permanent networks. Moreover, we show that the concentration-dependent yield stress of both

* Corresponding author: e-mail weitz@seas.harvard.edu.
[†] Harvard University.
[‡] Present address: FOM Institute for Atomic and Molecular Physics, Amsterdam, The Netherlands.
[§] Vrije Universiteit.

10.1021/ma070862l CCC: $37.00
Published on Web 09/20/2007

solutions and networks can be scaled onto similar master curves, allowing us to estimate a lower bound for the interaction force.

Materials and Methods

Materials. Tubulin is purified from bovine brain following standard procedures,[21] with two cycles of polymerization and depolymerization followed by removal of copurifying proteins on a phosphocellulose column. Biotinylated and fluorescently labeled tubulin are prepared by reacting tubulin with succinimidyl esters of biotin and Alexa 488.[21] The tubulin is labeled in polymeric form to protect residues important for microtubule assembly. Functional tubulin is selected after the labeling reaction by one cycle of polymerization and depolymerization. NeutrAvidin was purchased from Pierce Biotechnology (catalog no. 31000). NeutrAvidin is a protein with a molecular mass of 60 000 g/mol that forms a strong, practically irreversible bond with biotin, with a large binding affinity, K_a, on the order of 10^{15} M^{-1}.[22]

Concentration Determination. In the presence of guanosine triphosphate (GTP) and magnesium ions (Mg^{2+}), tubulin−GTP complexes assemble into microtubules. Microtubules are dynamic structures that fluctuate between assembly and disassembly. To suppress this dynamic instability we stabilize the microtubules with a nonhydrolyzable GTP analogue, guanosine 5′-[(α,β)-methylene]-triphosphate (GMPCPP).[23] Microtubules coexist with a temperature-dependent concentration of unpolymerized tubulin.[24] We measure the fraction of tubulin that is polymerized under our experimental conditions using a spectrophotometric assay. Microtubules are separated from unpolymerized tubulin by centrifugation and depolymerized in BRB buffer [80 mM piperazine-*N*,*N*′-bis(2-ethanesulfonic acid) (PIPES), 1 mM $MgCl_2$, 1 mM ethylene glycol bis(β-aminoethyl ether)-*N*,*N*,*N*′,*N*′-tetraacetic acid (EGTA), pH 6.8], containing 1 mM dithiothreitol (DTT), at 4 °C for 30 min. The tubulin concentration is determined by measuring the absorbance at a wavelength of 280 nm on a spectrophotometer. The absorbance is converted to molar concentration by use of an extinction coefficient of 115 000 M^{-1} cm^{-1}.[25] The molar concentration can be converted from weight concentrations via the molecular mass of the tubulin αβ-heterodimer of 110 000 g/mol (1 mg/mL tubulin corresponds to 9.1 μM). We find that at 35 °C virtually all tubulin is in polymerized form. When microtubules are kept at room temperature for 2 h, however, about 90% of the tubulin remains in polymeric form.

Microtubule Network Formation. Reconstituted microtubule networks are formed by mixing purified tubulin, 1 mM GMPCPP, 1 mM DTT, and tubulin polymerization BRB buffer. The solutions are immediately loaded in the rheometer and polymerized between the rheometer plates for 1 h at 35 °C. To form cross-linked networks, we use a two-step polymerization protocol. First, we copolymerize tubulin with biotin-labeled tubulin at 35 °C for 5 min. Next, we add the cross-link NeutrAvidin, load the solution in the rheometer, and wait for an hour. By variation of the tubulin concentration, c_T, the pore size of the networks can be changed. By variation of the molar concentration of biotin-labeled tubulin, c_B, relative to c_T, as well as the molar concentration of NeutrAvidin, c_N, relative to c_B, the degree of cross-linking can be varied. We define the molar ratios $R_B = c_B/c_T$ and $R_N = c_N/c_B$; these control the average distance between cross-links. We use both confocal microscopy[4] and multiple particle tracking[4,26] to estimate the pore size of the networks.

Microscopic and Image Analysis. Fluorescent images of single microtubule filaments are acquired on an epifluorescence microscope with a 100×, NA = 0.9, oil-immersion objective. Images of microtubule networks are obtained on a laser-scanning confocal microscope (Zeiss LSM 510) with a 60×, NA = 1.2, water-immersion objective and 488 nm laser light for excitation. Microtubules are polymerized from a mixture of tubulin and Alexa488-labeled tubulin at a 4:1 molar ratio. To quantify the pore size of the microtubule networks, we perform image analysis on 2D confocal slices.[27] We locate the microtubules by binary thresholding of the images. The threshold is determined as the mean intensity value plus 1 standard deviation. Pixels with intensity above the threshold are considered to be part of a microtubule. The number of those pixels with intensity larger than the threshold is counted per row and column. The distance between nearest-neighbor pixels within each row and column defines a pore size. We plot the distribution of the pore size in both *x* and *y* directions and fit it to an exponential, $P(\xi) = P_0 \exp(-r/\xi_0)$, where P_0 and the decay length, ξ_0, are fitting parameters. To obtain the distribution, we average about 100 images for each sample. We take the characteristic size, ξ, as a measure of the pore size.

Multiple Particle Tracking. Colloidal polystyrene beads of diameters, *a*, of 0.84, 1, and 2 μm are mixed with the tubulin solution so they are embedded in the microtubule networks, where they can probe the pore size. The spheres are coated with poly(L-lysine)-*graft*-poly(ethylene glycol) copolymer (PLL-*g*-PEG) to prevent protein adsorption.[28,29] The adsorption procedure is performed by following the protocol suggested by the manufacturer (SurfaceSolutionS). Microtubule/bead solutions are gently mixed and transferred into a glass chamber, made from a microscope slide and a coverslip with 1-mm-thick glass spacers and sealed with vacuum grease. We record the motions of particles at a rate of 30 frames/s using a fast digital camera (Phantom v7) with an exposure time of 260 μs. Roughly 100 particles are tracked for about 2 min. We calculate the mean-squared displacement of individual tracers, $\langle \Delta x^2(\tau) \rangle = \langle |x(t+\tau) - x(t)|^2 \rangle$, as a function of lag time τ, where the angular brackets indicate an average over many starting times, *t*. For $a < \xi$, the tracer particles are able to diffuse freely in the local pore at short times, whereas at longer times, their motion is restricted by the presence of the microtubule network. The plateau in the mean-squared displacement of individual particles at long times can therefore be viewed as a measure of the local constraining volume, or pore size, $\xi = a + [\langle \Delta x^2(\infty) \rangle]^{1/2}$, where $[\langle \Delta x^2(\infty) \rangle]^{1/2}$ is a measure of the distance between the particle surface and the pore wall.[26] The pore size distributions are fitted to a Poisson distribution to obtain a characteristic pore size.

Bulk Rheology. The mechanical response of the microtubule networks is measured with a stress-controlled rheometer (CVOR, Bohlin Instruments), with a 40-mm diameter stainless steel parallel plate geometry and a gap size of 120 μm. We use a solvent trap to prevent drying. Linear viscoelastic moduli are obtained by applying a frequency-dependent, sinusoidal stress, $\sigma(\omega)$, and measuring the resulting strain, $\gamma(\omega)$. To measure the mechanical response over a range of stresses, we measure the elastic modulus, $G'(\omega)$, and the viscous modulus, $G''(\omega)$, at a single frequency and vary the amplitude of the applied stress. Creep tests are used to study the mechanical behavior of the networks on longer time scales. A constant stress is applied for 100 s and then removed. The resultant displacement is measured during creep and subsequent recovery. In addition, we measure the behavior in the nonlinear regime with differential measurements. A small amplitude oscillatory stress, $\delta\sigma(\omega) \sim |\delta\sigma| e^{iwt}$, is superposed on a steady prestress, σ_0, and the oscillatory strain response, $\delta\gamma(\omega) \sim |\delta\gamma| e^{iwt}$, is measured. Provided the oscillatory stress is less than 10% of the steady prestress, the response is linear for all σ_0. The complex differential or tangent viscoelastic modulus is then given by $K^*(\omega,\sigma_0) = [\delta\sigma(\omega)/\delta\gamma(\omega)]|_{\sigma_0}$.

Results

Microscopic Structure of Microtubule Networks. Microtubules have a large bending rigidity, with a correspondingly large persistence length of a few millimeters,[1,2] which is about 100-fold larger than their contour length. Thus, to a good approximation, reconstituted microtubules behave as rigid rods. We dilute a solution of microtubules formed from 1 mg/mL tubulin by about 100-fold to obtain images of single filaments using epifluorescence microscopy, as shown in Figure 1A. We count the number of filaments of each length in bins of 0.2 μm width and plot the length distribution of more than 4000 single filaments in the inset of Figure 1B. The distribution is quite polydisperse and is well described by an exponent, as shown in Figure 1B. The characteristic filament length is $L = 2.6$ μm.

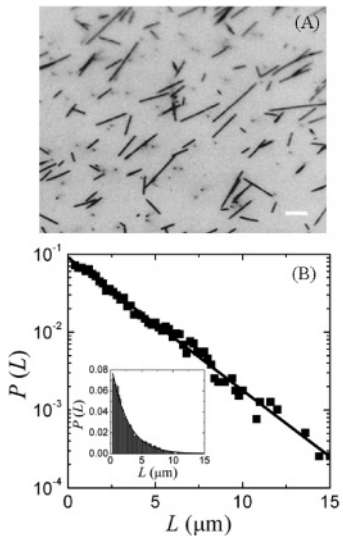

Figure 1. Length distribution of microtubules. (A) Epifluorescence microscopic images of dilute solutions of fluorescently labeled microtubules attached to a glass coverslip. Scale bar = 1 μm. (B) The microtubule length distribution, based on over 4000 filaments, follows an exponential decay with a characteristic length $L = 2.6$ μm, as highlighted by the semilog plot. A linear plot is shown in the inset.

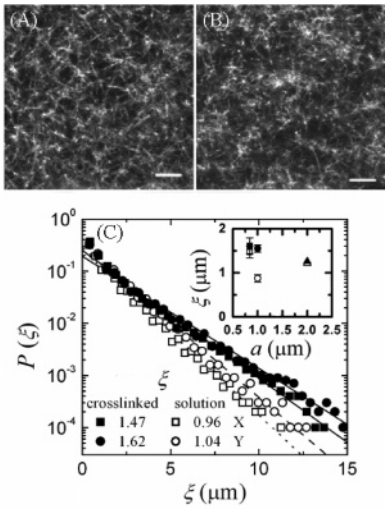

Figure 2. Two-dimensional confocal microscopy slices of fluorescently labeled networks of microtubules ($c_T = 1$ mg/mL). (A) Entangled network with a pore size of about 1 μm. (B) Cross-linked network with a pore size of about 1.5 μm. Scale bar = 5 μm. (C) Pore size distribution measured by analysis of confocal images. (Inset) Pore sizes of microtubule solutions (open symbols) and networks (solid symbols) obtained by particle tracking using probe particles of different diameters, a.

Solutions of entangled microtubules form isotropic and homogeneous networks, as shown by the confocal micrograph in Figure 2A. Over the complete tubulin concentration range studied (0.5−5 mg/mL), there is no apparent liquid crystalline structure, consistent with previous work reporting alignment only above tubulin concentrations of 5.5 mg/mL.[30] Upon cross-linking of biotinylated microtubules with NeutrAvidin, a tetravalent cross-link of biotin, the networks become somewhat inhomogeneous and the characteristic mesh size, measured from the confocal images, increases slightly in both x and y directions, as shown in Figure 2B.

We can predict a mesh size ξ from the tubulin concentration using simple geometrical arguments.[31] We assume that the network is homogeneous and the microtubules are rigid rods arranged on a cubic lattice. For a given mass of tubulin

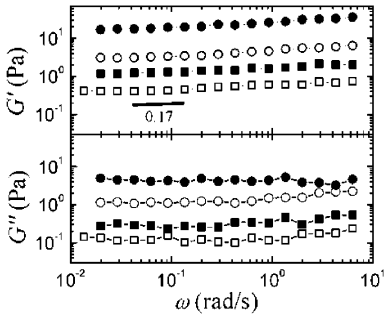

Figure 3. Linear viscoelastic shear moduli of entangled microtubule solutions (open symbols) and cross-linked networks (solid symbols) for $c_T = 1$ mg/mL (squares) and 5 mg/mL (circles). The elastic modulus, G', dominates over the viscous modulus, G''. The elastic moduli exhibit a rather weak power law scaling with frequency ω, with an exponent of 0.14 for cross-linked networks and 0.17 for entangled solutions. The cross-linked networks are 3−6 times stiffer than the solutions.

monomers per unit length of microtubule, ρ_L, and tubulin mass per unit volume, c_T, the total filament length per unit volume is given by the ratio c_T/ρ_L. The total filament length per mesh volume, ξ^3, is then 3ξ. Thus, the mesh size ξ can be written as

$$\xi = \sqrt{\frac{3\rho_L}{c_T}} \tag{1}$$

Microtubules are formed with 13 protofilaments, with a diameter given by the tubulin monomer size of about 5 nm and mass of 55 kD. Therefore, $\xi \approx 0.89/\sqrt{c_T}$ (μm), where c_T is in units of mg/mL. We can compare these estimated pore sizes with the values measured by analysis of confocal images. The characteristic values are about 1 μm for microtubule solutions and 1.5 μm for cross-linked networks, as shown in Figure 2C. We also determine ξ by multiple particle tracking. We find similar values, 1.2 μm for microtubule solutions and 1.7 μm for cross-linked networks, as shown in the inset of Figure 2C. Mesh sizes measured with multiple particle tracking are inherently somewhat larger than those measured by confocal imaging.[4] Confocal microscopy underestimates the pore size, because randomly cut cross-sections of a 3D object are smaller than the maximum pore diameter, while multiple particle tracking overestimates the mesh size, since it does not measure pores smaller than the particle size. Nevertheless, there is good agreement between the values measured with two independent techniques, and both are consistent with the predicted values. Analysis of Fourier transforms of the confocal images gives similar values for the characteristic length scales, namely, 2.0 μm for microtubule solutions and 2.6 μm for cross-linked microtubule networks.

Linear Rheology of Microtubule Networks. We polymerize microtubule networks *in situ* between the plates of the rheometer. After polymerization, we measure the linear viscoelastic moduli by small amplitude oscillatory stress measurements with strains of less than 0.05. The elastic modulus, G', of both microtubule solutions and cross-linked networks always dominates the viscous modulus, G'', across the full experimental frequency range, as shown in Figure 3; this indicates that the networks are predominantly elastic. The moduli depend only very weakly on frequency, with an approximately power-law scaling of the elastic modulus, $G' \sim \omega^\beta$, with $\beta = 0.17$ for microtubule solutions.

We examine the effect of cross-linking by incorporating a fraction of biotinylated tubulin into the microtubules and adding NeutrAvidin, a tetravalent permanent cross-link of biotin. We tune the molar concentration of biotin-labeled tubulin, c_B, as

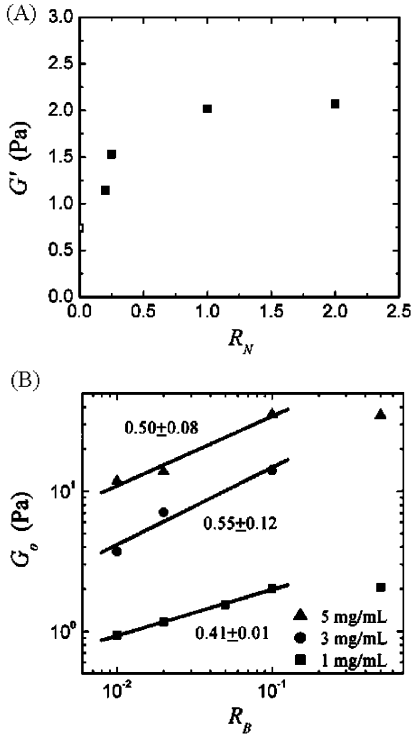

Figure 4. (A) Linear elastic modulus of cross-linked microtubule networks at a fixed tubulin concentration ($c_T = 1$ mg/mL) and different NeutrAvidin/biotin ratios. Below a molar ratio of NeutrAvidin:biotin of 0.25, G' increases with R_N, ultimately saturating at $R_N = 1$. **(**B**)** G_0 shows power-law scaling in the molar ratio of biotin-labeled tubulin to tubulin, R_B, with $G_0 \sim R_B^{0.5}$, for three tubulin concentrations.

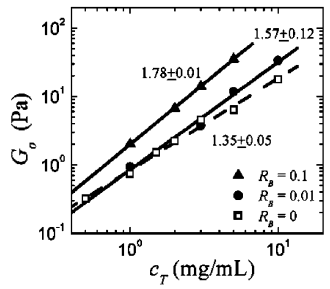

Figure 5. Dependence of the linear elastic modulus on microtubule concentration, c_T, and cross-link density, R_B. G_0 scales as a power law in c_T, with an exponent of 1.6−1.8 for cross-linked networks and 1.4 for solutions.

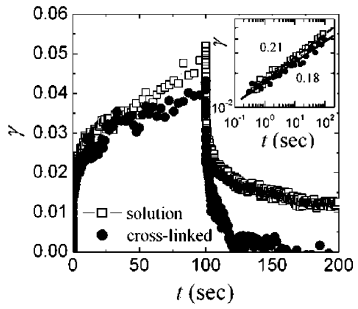

Figure 6. Creep test for microtubule solutions and cross-linked networks. We apply a constant stress of 0.04 Pa for 100 s and measure the resultant strain, γ. The strain evolves as a power law (see inset). Upon removal of the stress, the entangled networks have a residual strain of 0.012, whereas the strain of cross-linked networks recovers to nearly zero.

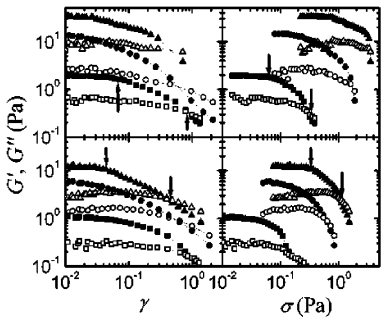

Figure 7. Oscillatory measurements of G' (solid symbols) and G'' (open symbols) at large amplitudes of applied strain and stress for microtubule networks (A, upper left, and B, upper right) and solutions (C, lower left, and D, lower right) for $c_T = 1$ mg/mL (squares), 3 mg/mL (circles), and 5 mg/mL (triangles). The critical stress and strain are the onset of the nonlinear elastic response, and the yield stress and strain are defined as the stress and strain where G' equals G'', as shown by the arrows. The elastic modulus is linear up to a maximum strain of ~0.1, and the networks yield at maximum strain of ~0.9 (for $c_T =$ 1 mg/mL).

well as the NeutrAvidin concentration, c_N, for a fixed tubulin concentration, c_T, such that the density of cross-links, expressed as molar ratios $R_B = c_B/c_T$ and $R_N = c_N/c_B$, varies. At fixed c_T and c_B, $G'(\omega)$ increases rapidly with R_N and saturates at $R_N =$ 1, as shown in Figure 4A; we therefore fix $R_N = 1$ in all cross-linked samples. Upon cross-linking, the elastic modulus still dominates the viscous modulus, as shown by the solid symbols in Figure 3. The elastic modulus again depends weakly on frequency with a power-law dependence with an exponent of about 0.14. The elastic modulus can be varied by changing either the tubulin concentration or the degree of cross-linking. Since the elastic modulus is only weakly dependent on frequency, we can characterize the network elasticity with a single elastic plateau modulus, G_0. For cross-linked networks, the plateau storage modulus exhibits a scaling $G_0 \sim R_B^{0.5}$ for three values of c_T, as shown in Figure 4B; G_0 increases more than 3-fold when R_B increases from zero to 0.1 at $c_T = 1$ mg/mL and 6-fold when $c_T = 5$ mg/mL, as shown in Figures 3 and 4B. Saturation of G_0 is expected when the distance between cross-linking points becomes comparable to the mesh size. Moreover, the elastic modulus exhibits a power law scaling with tubulin concentration, $G_0 \sim c_T^{\nu}$, with $\nu = 1.4$ for solutions and 1.6−1.8 for permanently cross-linked networks, as shown in Figure 5. We study the mechanical behavior at longer times by creep tests, where we apply a constant stress for 100 s and measure the resultant strain. The strain exhibits a power-law increase with time, $\gamma(t) = t^{\alpha}$, with $\alpha = 0.21$ for microtubule solutions and $\alpha = 0.18$ for cross-linked networks, as shown in Figure 6 and its inset. These weak power laws are consistent with the frequency dependence observed in the dynamic measurements. Upon removal of the stress, the strain recovers to nearly zero for cross-linked networks, which is characteristic of stably cross-linked gels.[32] In contrast, microtubule solutions do not fully recover on the experimental time scale, having a residual strain of 0.012.

Nonlinear Rheology of Microtubule Networks. We probe the nonlinear elastic behavior of the microtubule networks by large amplitude oscillatory stress measurements. The linear regime for all cross-linked networks is small, extending only up to $\gamma \sim 0.1$, as shown in Figure 7A. As the stress increases further, the modulus of the networks starts to decrease with increasing stress amplitude σ, as shown in Figure 7B. The microtubule solutions have a very similar response to cross-linked networks, as shown in Figure 7C,D. We characterize the onset of the nonlinear elastic response by the critical stress and

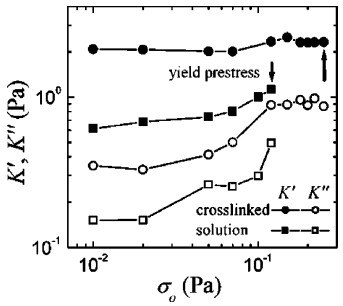

Figure 8. Differential elastic modulus, K', and viscous modulus, K'', of microtubule networks, obtained by applying a constant prestress, σ_0, and measuring the deformation in response to an additional oscillatory stress. The system yields at a prestress of 0.12 Pa for the 1 mg/mL tubulin solution and 0.25 Pa for the cross-linked network at the same c_T.

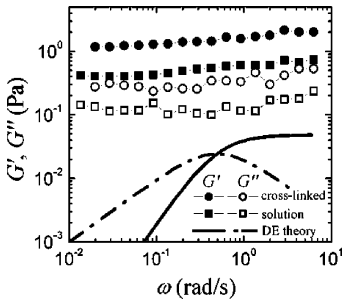

Figure 9. Comparison of measured linear moduli of microtubule solutions ($c_T = 1$ mg/mL) with the Doi−Edwards model predictions. The measured elastic modulus (■) is more than 10-fold higher than the theoretical expectation (—); moreover, no terminal relaxation is observed, while the theory predicts a time scale of tens of seconds. For cross-linked networks, our data (circles) are much smaller than the simple effective medium model derived in the limit of high cross-link densities, where $G' \sim 10^4$ Pa.

define the yield stress as the stress where G' equals G'', as shown by the arrows in Figure 7.

To further explore the stress weakening in the nonlinear regime, we measure the differential or tangent elastic modulus at a tubulin concentration of 1 mg/mL. The yield prestress is determined from the point where the tangential elastic modulus becomes smaller than the viscous modulus. The networks yield at a very small stress of 0.12 Pa for microtubule solutions and 0.25 Pa for cross-linked networks, as shown in Figure 8. This observation is consistent with the yield stress found in the large amplitude oscillatory stress tests, where we find a yield stress of 0.1 Pa for solutions and 0.3 Pa for cross-linked networks.

Discussion

Microtubule networks are soft viscoelastic materials with an elastic modulus that dominates the viscous modulus over the experimental frequency range of 0.01−6 rad/s. Upon addition of an increasing amount of permanent cross-links, the elastic modulus initially increases, but it saturates when the distance between cross-linking points becomes comparable to the distance between entanglement points. In the linear viscoelastic regime, cross-linked networks have larger shear moduli than microtubule solutions. Moreover, the modulus of cross-linked networks depends somewhat more strongly on tubulin concentration than that of solutions. There is no evidence of terminal relaxation for either the solutions or the cross-linked networks. This suggests that it takes longer than 600 s for microtubules to reptate and release the stress, which is consistent with previous observations.[8]

The concentration dependence of the elastic modulus of microtubule solutions and networks is slightly weaker than for those of actin filaments. For filamentous actin, the elastic modulus scales as a power-law in actin concentration with exponents of $\nu = 1.4$ for solutions[33−35] and $\nu = 2.2-2.5$ for cross-linked networks.[5,36,37] Actin filaments and microtubules have a very different bending rigidity; while actin filaments have a persistence length of about 20 μm, microtubules have a persistence length of a few millimeters.[1,2] Thus, actin filaments are well described as semiflexible filaments, whereas microtubules are much better approximated as rigid rods.

The elastic properties of rigid rod systems are generally interpreted in terms of the Doi−Edwards model.[20] This model assumes that the rods are rigid, noninteracting, and of uniform length. Solutions of slender rodlike polymers are classified into four concentration regimes based on the number density of rods, namely, dilute, semidilute, concentrated isotropic, and nematic. The concentrations of tubulin in our experiments correspond to the region near the onset of semidilute solutions, since the contour lengths L are somewhat larger than the mesh size ξ. In the semidilute regime, longitudinal diffusion of microtubules is virtually unhindered, while transverse diffusion is severely limited by neighboring microtubules and thus the perpendicular friction is infinite. This characteristic feature is modeled as a fictitious tube surrounding each microtubule. When the network is slightly deformed, the rod orientations are affected. Stress relaxation is thus determined by rotational diffusion of the rods. The relaxation time corresponds to the time scale on which the direction of the rod's principal axis changes. Rod reorientation occurs gradually by a "reptation"-like sequence of longitudinal translational motions over a typical length scale L. On short time scales, the rod suspension is predominantly elastic, whereas at long times, after full structural relaxation, the suspension is viscous. By use of this "tube" model, the rotational relaxation time can be estimated as $\tau_r = 1/6D_r$, where D_r is the rotational diffusion of the rods, $D_r = \beta D_{r,0}(\nu L^3)^{-2}$, $D_{r,0}$ is the rotational diffusion of the rods in a dilute solution, ν is the number density of rods, and β is a numerical factor. For a small deformation, the complex viscosity is

$$\eta^*(\omega) = 3\nu k_B T \frac{\tau_r}{1 + i\omega\tau_r} \qquad (2)$$

The Doi−Edwards model thus predicts a linear increase of the elastic modulus with the concentration of rods. We can directly compare the magnitude of the elastic modulus with the predictions of eq 2, assuming a mean microtubule length of 2.6 μm. The precise value of β is not known. Here we choose $\beta = 1$ to obtain an estimate of the upper bound of the moduli and relaxation time. The microtubule solutions are more than 10-fold stiffer than theoretically expected, as shown in Figure 9. Moreover, we do not observe terminal relaxation on the experimental time scale of 600 s, while the theory predicts a time scale of only tens of seconds. There is also a discrepancy in the concentration dependence of the linear elastic modulus. As shown in Figure 5, our data have a significantly stronger concentration dependence than the linear increase predicted by the model. We therefore conclude that the Doi−Edwards model cannot explain our data.

For cross-linked networks, we compare the elastic plateau modulus with a simple effective medium model derived in the limit of high cross-link densities,[38,39] $G_0 \sim {}^1/_{15}\rho\mu$, where μ is the stretch modulus of filaments and ρ is the spatial density (length per volume) of filaments. Since $\mu \sim E\pi r^2$, where E is the Young's modulus and r is the microtubule radius, and $\rho \approx 1.7 \times 10^{12}$ m^{-2} in solutions of 1 mg/mL, we find $G_0 \sim 10^4$ Pa.

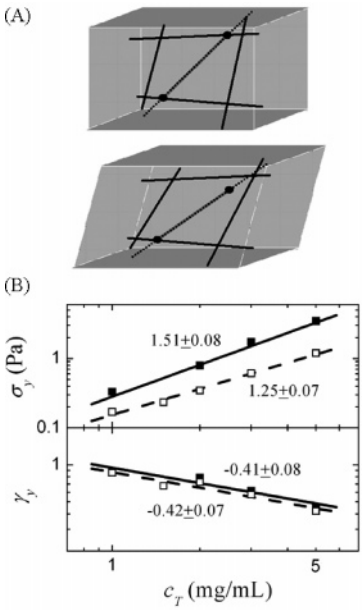

Figure 10. (A) Schematic of a network of rods. Under shear, induced tension in the central rod segment is borne by the cross-links shown as black circles. If the resulting force on the cross-link exceeds a maximum *f*, the cross-link is assumed to break (as shown for the upper cross-link). At this point of rupture, the shear stress is proportional to the concentration of rod segments (specifically, the density $\sim 1/\xi^2$ of rods per unit area in a shear plane, shown in dark gray), as well as the average number of cross-links per filament ($\sim L/\xi$). (B) Dependence of the yield stress and strain, σ_y and γ_y, of both microtubule solutions and cross-linked networks on tubulin concentration; $\sigma_y \sim c_T^{1.51}$ for cross-linked networks, and $\sigma_y \sim c_T^{1.25}$ for solutions; whereas, by contrast, γ_y is indistinguishable for solutions and cross-linked networks, and scales as $c_T^{-0.42}$.

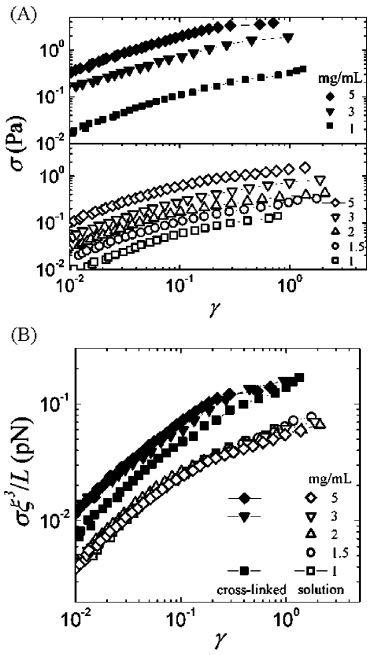

Figure 11. (A) Dependence of σ on γ at 0.6 rad/s for both microtubule solutions (open symbols) and cross-linked networks (solid symbols) for various concentrations of tubulin. For all concentrations, σ increases linearly with γ up to $\gamma = 0.1$ and reaches a plateau. **(**B**)** Master curves of scaled σ versus γ where the stress is scaled by ξ^3/L.

As shown in Figure 9, this value is much larger than our experimental data; moreover, this model predicts a linear concentration dependence of G_0, which is different from our experimental observation. This model therefore also fails to explain the viscoelastic response of cross-linked microtubule networks, perhaps due to the fact that the contour length is not sufficient to form many cross-links per filament.[40]

Given the large discrepancy between our data and the predictions for noninteracting rigid rods, as well as the similarities between the rheological responses of microtubule solutions and cross-linked networks, we suspect that there are weak attractive interactions, cross-links, or bonds between the microtubules. We develop a simple model to estimate this hypothetical interaction force, inspired by recent work on carbon nanotubes.[41,42] We assume for simplicity that whenever two filaments cross, there is an interaction at the intersection point. In the presence of a shear stress, filaments are displaced relative to their neighbors, disrupting these interactions. At the yield stress, most interfilament interactions are broken; every intersection can thus be assumed to contribute an average tension, *f*, to a single filament, as sketched in Figure 10A. The yield stress, σ_y, of networks is then approximately

$$\sigma_y \cong \frac{f}{\xi^2}\frac{L}{\xi} \tag{3}$$

where L/ξ is the number of intersections per filament. Since $\xi \sim c_T^{-1/2}$, we predict that the concentration dependence of the yield stress is $\sigma_y \sim c_T^{3/2}$. Our data are reasonably consistent with this prediction, as shown in Figure 10B for both microtubule solutions and cross-linked networks. For all tubulin concentrations, the stress−strain data measured at 0.6 rad/s exhibits a linear increase of stress with strain up to $\gamma = 0.1$, whereupon it reaches a plateau, as shown in Figure 11A. This plateau indicates the yield event. This type of analysis has been used to infer the attractive interactions in colloidal gels[43] and carbon nanotube suspensions.[41] In order to infer the interaction strength between microtubules, we can eliminate the concentration dependence from the stress. The viscoelastic response of microtubule solutions and cross-linked networks can be collapsed onto two separate master curves by scaling the stress by a factor of ξ^3/L, as shown in Figure 11B. The plateau of the scaled stress corresponds to the strength of the interaction per intersection point.

We find small values for the force, 0.06 pN for solutions and 0.15 pN for cross-linked networks. However, for a number of reasons these values are likely underestimations. First, we assumed that every intersection point contributes a tension to the filament, so that the distance between interaction points is comparable to the mesh size. In reality, it is very unlikely that all intersection points are interacting. Second, in three dimensions the mesh size represents the average distance between points of closest approach and not points of contact. Therefore, the distance between interaction points is likely larger than the mesh size. Since the interaction force is proportional to the cube of this distance, the "effective" mesh size of interaction points has a dramatic effect on the value of the force. Third, the mesh sizes of microtubule solutions and cross-linked networks were assumed to be the same and to depend only on tubulin concentration. However, both confocal image analysis and multiple particle tracking indicate a larger mesh size for the cross-linked networks. This factor also results in an underestimate of the interaction force in cross-linked networks. Finally, we assumed a homogeneous deformation with an average force that is equally distributed over all filaments. However, the yield strain of networks is around 0.9, so the network deformation is likely highly nonaffine, with a distribution of forces. Since the force that is actually responsible for yielding the network is larger than the assumed mean force, the actual interaction

strength is underestimated in this model. Thus we believe that the actual yield forces are higher than the values we obtain.

Weak cross-linking in our solutions could result from low-affinity, nonspecific interactions, a small concentration of residual microtubule-associated proteins (MAPs), or a small fraction of denatured tubulin. Such weak attractions can explain why microtubule solutions have a larger plateau modulus and longer relaxation time than predicted by the Doi−Edwards model. Moreover, it suggests the yield events of networks are due to the breakage of some interactions for both microtubule solutions and cross-linked networks. Creep tests, such as those shown in Figure 6, exhibit a residual strain for microtubule solutions, thereby strongly suggesting that cross-linking effects are weak and transient, if present at all. Calorimetry measurements, small-angle X-ray scattering (SAXS), or freeze−fracture electron microscopy could be used in the future to independently confirm the existence of attractive interactions. Both solutions and cross-linked networks show strain weakening and yield irreversibly at very small stresses on the order of 10^{-1} Pa. This strain-weakening behavior is consistent with an earlier report of shear-thinning of microtubule networks under an applied steady shear stress.[44] This strain-weakening response distinguishes microtubule networks from other cytoskeletal protein networks, which tend to display strong strain stiffening.[5] This difference is likely due to the much larger bending rigidity of microtubules compared to that of actin and intermediate filaments.[1,2] Since the contour length of our reconstituted microtubules is a few micrometers, much smaller than the persistence length (millimeters), there are no thermal fluctuations to pull out when strained. Therefore, entropic stretching is not expected in microtubule networks.

Conclusions

We measured linear and nonlinear viscoelastic properties of microtubule solutions and cross-linked networks in the semidilute concentration regime over a wide frequency range. Microtubule networks are an interesting model system for rigid rodlike polymers of high aspect ratio. Microtubule solutions are more elastic than predicted for noninteracting rods, which we believe is explained by the presence of weak interactions between the filaments. On the basis of a simple model, we can estimate these interaction forces. The highly nonaffine deformation at large yield strains remains a challenging problem for further theoretical investigations, since existing mean-field approaches do not apply. Our data provide a framework to understand the rheological consequences of adding microtubule-associated cross-linking and motor proteins, and ultimately the mechanical behavior of the composite cytoskeleton of actin, intermediate filaments, and microtubules that determines mechanics of living cells.

Acknowledgment. We thank D. J. Needleman for assistance with tubulin purification. This work was supported by the NSF (DMR-0602684 and CTS-0505929), the Harvard MRSEC (DMR-0213805), and FOM/NWO. G.H.K. is supported by a European Marie Curie Fellowship (FP6-2002-Mobility-6B, Contract 8526).

References and Notes

(1) Gittes, F.; Mickey, B.; Nettleton, J.; Howard, J. *J. Cell Biol.* **1993**, *120* (4), 923−934.
(2) Brangwynne, C. P.; Koenderink, G. H.; MacKintosh, F. C.; Weitz, D. A. *Biophys. J.* **2007**, *93* (1), 346−359.
(3) Alberts, B.; Johnson, A.; Lewis, J.; Raff, M.; Roberts, K.; Walter, P. *Molecular Biology of The Cell*, 4th ed.; Garland Science: New York, 2002.
(4) Shin, J. H.; Gardel, M. L.; Mahadevan, L.; Matsudaira, P.; Weitz, D. A. *Proc. Natl. Acad. Sci. U.S.A.* **2004**, *101* (26), 9636−9641.
(5) Gardel, M. L.; Shin, J. H.; MacKintosh, F. C.; Mahadevan, L.; Matsudaira, P.; Weitz, D. A. *Science* **2004**, *304* (5675), 1301−1305.
(6) Dogterom, M.; Yurke, B. *Science* **1997**, *278* (5339), 856−860.
(7) Dogterom, M.; Janson, M. E.; Faivre-Moskalenko, C.; Horst, A. v. d.; Kerssemakers, J. W. J.; Tanase, C.; Mulder, B. M. *Appl. Phys. A: Mater. Sci. Process.* **2002**, *75* (2), 331−336.
(8) Janmey, P. A.; Euteneuer, U.; Traub, P.; Schliwa, M. *J. Cell Biol.* **1991**, *113* (1), 155−160.
(9) Sato, M.; Schwartz, W. H.; Selden, S. C.; Pollard, T. D. *J. Cell Biol.* **1988**, *106* (4), 1205−1211.
(10) Enomoto, H.; Einaga, Y.; Teramoto, A. *Macromolecules* **1985**, *18* (12), 2695−2702.
(11) Takada, Y.; Sato, T.; Teramoto, A. *Macromolecules* **1991**, *24* (23), 6215−6219.
(12) Wierenga, A. M.; Philipse, A. P. *J. Colloid Interface Sci.* **1996**, *180* (2), 360−370.
(13) Graf, C.; Kramer, H.; Deggelmann, M.; Hagenbuchle, M.; Johner, C.; Martin, C.; Weber, R. *J. Chem. Phys.* **1993**, *98* (6), 4920−4928.
(14) Schmidt, F. G.; Hinner, B.; Sackmann, E.; Tang, J. X. *Phys. Rev. E* **2000**, *62* (4), 5509−5517.
(15) Kiss, G. K.; Porter, R. S. *J. Polym. Sci.: Polym. Phys. Ed.* **1980**, *18*, 361−388.
(16) Lee, H. C.; Brant, D. A. *Macromolecules* **2002**, *35* (6), 2212−2222.
(17) Rogers, S. S.; Venema, P.; van der Ploeg, J. P. M.; van der Linden, E.; Sagis, L. M. C.; Donald, A. M. *Biopolymers* **2006**, *82* (3), 241−252.
(18) Lee Briehl, R. W.; Guzman, A. E. *Blood* **1994**, *83* (2), 573−579.
(19) Tadmor, R.; Khalfin, R.; Cohen, Y. *Langmuir* **2002**, *18* (19), 7146−7150.
(20) Doi, M.; Edwards, S. F. *The Theory of Polymer Dynamics*; Clarendon Press: Oxford, U.K., 1988.
(21) Protocols from Professor Tim Mitchison's laboratory at Harvard University Medical School.
(22) Hiller, Y.; Gershoni, J. M.; Bayer, E. A.; Wilchek, M. *Biochem. J.* **1987**, *248* (1), 167−171.
(23) Hyman, A. A.; Salser, S.; Drechsel, D. N.; Unwin, N.; Mitchison, T. *Mol. Biol. Cell* **1992**, *3* (10), 1155−1167.
(24) Fygenson, D. K.; Braun, E.; Libchaber, A. *Phys. Rev. E* **1994**, *50* (2), 1579−1588.
(25) Detrich, H. W.; Williams, R. C. *Biochemistry* **1978**, *17* (19), 3900−3907.
(26) Valentine, M. T.; Kaplan, P. D.; Thota, D.; Crocker, J. C.; Gisler, T.; Prud'homme, R. K.; Beck, M.; Weitz, D. A. *Phys. Rev. E* **2001**, *64* (6), 061506.
(27) Kaufman, L. J.; Brangwynne, C. P.; Kasza, K. E.; Filippidi, E.; Gordon, V. D.; Deisboeck, T. S.; Weitz, D. A. *Biophys. J.* **2005**, *89* (1), 635−650.
(28) Kenausis, G. L.; Voros, J.; Elbert, D. L.; Huang, N.; Hofer, R.; Ruiz-Taylor, L.; Textor, M.; Hubbell, J. A.; Spencer, N. D. *J. Phys. Chem. B* **2000**, *104* (14), 3298−3309.
(29) Pasche, S.; DePaul, S. M.; Voros, J.; Spencer, N. D.; Textor, M. *Langmuir* **2003**, *19* (22), 9216−9225.
(30) Hitt, A. L.; Cross, A. R.; Williams, R. C., Jr. *J. Biol. Chem.* **1990**, *265* (3), 1639−1647.
(31) de Gennes, P. G.; Pincus, P.; Velasco, R. M.; Brochard, F. *J. Phys.* **1976**, *37* (12), 1461−1473.
(32) Janmey, P. A.; Hvidt, S.; Lamb, J.; Stossel, T. P. *Nature* **1990**, *345* (6270), 89−92.
(33) Hinner, B.; Tempel, M.; Sackmann, E.; Kroy, K.; Frey, E. *Phys. Rev. Lett.* **1998**, *81* (12), 2614−2617.
(34) Morse, D. C. *Phys. Rev. E* **1998**, *58* (2), R1237−R1240.
(35) Maggs, A. C. *Phys. Rev. E* **1997**, *55* (6), 7396−7400.
(36) MacKintosh, F. C.; Käs, J.; Janmey, P. A. *Phys. Rev. Lett.* **1995**, *75* (24), 4425−4428.
(37) Tharmann, R.; Claessens, M. M. A. E.; Bausch, A. R. *Phys. Rev. Lett.* **2007**, *98* (8), 088103.
(38) Gittes, F.; MacKintosh, F. C. *Phys. Rev. E* **1998**, *58* (2), R1241−R1244.
(39) Morse, D. C. *Macromolecules* **1998**, *31* (20), 7044−7067.
(40) Head, D. A.; Levine, A. J.; MacKintosh, F. C. *Phys. Rev. Lett.* **2003**, *91* (10), 108102.
(41) Hough, L. A.; Islam, M. F.; Janmey, P. A.; Yodh, A. G. *Phys. Rev. Lett.* **2004**, *93* (16), 168102.
(42) Hobbie, E. K.; Fry, D. J. *Phys. Rev. Lett.* **2006**, *97* (3), 036101.
(43) Russel, W. B.; Saville, D. A.; Schowalter, W. R. *Colloidal Dispersions*; Cambridge University Press: Cambridge, U.K., 1989.
(44) Buxbaum, R. E.; Dennerll, T.; Weiss, S.; Heidemann, S. R. *Science* **1987**, *235* (4795), 1511−1514.

MA070862L